Broadband Achromatic Metalens in the Long-Wave Infrared Regime

Yongjian Zheng, Shaonan Zheng, Yuan Dong, Lianxi Jia, Qize Zhong, Yuandong Gu, and Ting Hu

***Abstract*—Compared with conventional lenses, metalenses can offer smaller form factor, light weight and new functionality, and have become the focus of the recent investigations of metasurface. To date, quite a lot of studies have been reported for chromatic aberration correction of metalenses. Noting most work was carried out to satisfy the required group delay or dispersion by introducing sophisticated and integrated nanopillars, which are obtained using computationally intensive global search algorithms. Generally, the design is time-consuming. Here, we propose an alternative scheme, where metalens that corrects the chromatic aberration can be designed by optimizing the spectral degree of freedom C(ω), rather than relying on time-consuming algorithms. The proposed metalens is compatible with the complementary metal oxide semiconductor (CMOS) fabrication process. The numerically demonstrated metalens with a diameter of 200 μm and a numerical aperture (NA) of 0.24 has a small focal length fractional change (FLFC) of 4.1% over the wavelength of 9∼12 μm with an average efficiency of 51.7% in transmission mode. Moreover, the effect of fabrication deviations on the performance of the metalens is analyzed, showing critical dimension (CD) bias, sidewall angle and pillar height all have different levels of influence on the performance of the metalens.**

***Index Terms*—Metasurface, metalens, achromatic focusing, long-wave infrared (LWIR).**

I. Introduction

DISPERSION is one of the important properties of optical materials, which is particularly important in designing optical components and systems. While, the chromatic aberration caused by material dispersion in optical imaging will adversely affect the imaging system and even seriously affect the imaging quality. Traditional optical systems often need to combine materials with different refractive indices to eliminate chromatic aberration. Although this approach eliminates chromatic aberrations, it increases the complexity of the system, which is disadvantageous for the miniaturizations of the system. Long-wave infrared (LWIR) is crucial for a variety of applications such as environmental sensing and medical imaging [1], [2]. LWIR lens is one of the most basic and important components in an infrared imaging system. Conventional LWIR optics are bulky and heavy compared to their visible and near-infrared counterparts, which limits their miniaturization applications.

Metasurfaces composed of sub-wavelength meta-atom units enable optical components into thin, planar, multifunctional elements and they can dramatically reduce device size and system complexity [3], [4], [5], [6], [7], [8], [9]. Many metasurface applications have been reported such as holography [10], [11], [12], metalenses [13], [14], [15], [16], metasurface cloak [17], and vortex beam generation [18], [19], [20]. As one of the most important applications of metasurfaces, metalenses typically suffer from chromatic aberration due to material dispersion and diffraction of light [21], [22]. Chromatic aberration limits the use of metalenses in many scenarios including color imaging. Much effort has been devoted to solving this problem and developing achromatic focusing metalens in the visible [22], [23], [24], [25], [26], [27], [28], [29], [30], [31], near-infrared [21], [32], [33], [34], [35], [36], [37], [38], [39], [40], [41], [42], and mid-infrared (MIR) spectrums [43], [44]. Numerous studies have been reported for multi-wavelength achromatic metalenses [35], [36], [37], [38], [39], but the application of achromatic metalenses with continuous broadband regime is more common in practice. An alternative approach to correct the achromatic aberration is to use multi-layers or hybrid metasurfaces, while this approach raises even greater requirements on fabrication process [29], [39], [40]. Other reported achromatic metalenses use complex structures or integrated nanopillars to construct metalenses [25], [26], [27], [28], [31], [40], [41], [42], where extensive parameter sweeps are required to find suitable structures during the process of building the structure library, which relies on computationally intensive global search algorithms. It should be also noted the dispersion of the meta-atom unit would deviate from the calculated dispersion in building block due to the different surrounding units in the metalens, weakening the achromatic correction.

Here, we propose a scheme, where the proposed achromatic metalens in the long-wave infrared regime of 9∼12 μm is designed by optimizing the spectral degree of freedom C(ω). The combination of the adjacent pillars, which can be considered as a supercell will redistribute when C(ω) is changed. C(ω) provides one more dimension to optimize the group delay of the metalens to suppress the achromatic aberration, which hasn't been discussed before. The achromatic metalens with a diameter of 200 μm and NA of 0.24 is proposed to fabricate on all-silicon wafer

Manuscript received 14 December 2022; revised 6 January 2023; accepted 4 February 2023. Date of publication 9 February 2023; date of current version 21 February 2023. This work was supported by the Open Fund of Key Laboratory of Advanced Display and System Applications of Ministry of Education (Shanghai University). *(Corresponding author: Qize Zhong.)*

Yongjian Zheng, Shaonan Zheng, Yuan Dong, Qize Zhong, Yuandong Gu, and Ting Hu are with the School of Microelectronics, Shanghai University, Shanghai 201800, China (e-mail: 2072zyj@shu.edu.cn; snzheng@shu.edu.cn; dongyuan@shu.ed.cn; zhongqize@shu.edu.cn; alex.gu@shu.edu.cn; hu-t@shu.edu.cn).

Lianxi Jia is with the School of Microelectronics, Shanghai University, Shanghai 201800, China, and also with the Shanghai Institute of Microsystem and Information Technology, Shanghai 200050, China (e-mail: jialx@shu.edu.cn).

Digital Object Identifier 10.1109/JPHOT.2023.3243409

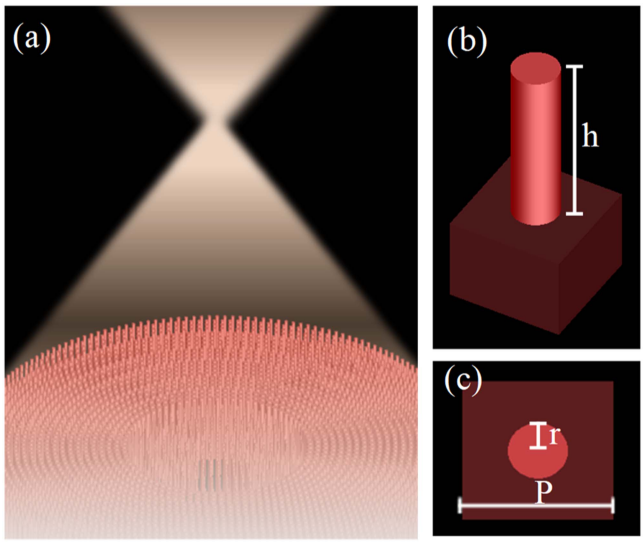

Fig. 1. (a) Schematic of a focusing metalens. (b) the meta-atom consists of a silicon nanopillar with height h = 7.9 μm on a silicon substrate. (c) the top view of the meta-atom. The period p = 3.05 μm.

using CMOS-compatible process. To evaluate the performance of the achromatic metalenses, the focal length fractional change (FLFC) and chromatic focal shift are discussed. Moreover, we also analyze the effect of fabrication process deviation on the performance of the metalens. The proposed scheme offers perspectives to extend the operating bandwidth of achromatic metalenses to LWIR and we can envision applications in miniaturized and integrated LWIR imaging.

II. Design Principle and Result

Traditional lenses composed of glass or other transparent materials rely on the accumulation of optical path in the medium to achieve phase control. Similar with a refractive lens and other diffractive optical lens, the relative phase profile for metalenses to achieve focusing can be expressed as follows:

$$\varphi(r,\omega) = \mathrm{C}(\omega) - \frac{\omega}{c}\left(\sqrt{r^2+f^2} - f\right), \tag{1}$$

where ω, C(ω), c, r, and f are angular frequency, spectral degree of freedom, speed of light, radial coordinate and focal length, respectively. C(ω) is related with central design wavelength, which can be set in a range of 0 to 2π. The relative phase profile doesn't change as C(ω) takes on a different value for a given design frequency. The required phase of the metalens is controlled by the shape and geometry of the meta-atom unit. One of the important processes in designing metalenses is to design a libary of the structures, such as diameter, to achieve a phase coverage of 0$\sim$2π. The meta-atom unit of our metalens shown in Fig. 1(b) is a circular silicon pillar on a silicon substrate. These pillars are regarded as truncated waveguides. Different phase responses can be obtained by engineering the diameter of the nanopillars. Due to the dispersive properties of materials, effective refractive indices vary with different wavelengths for the same structure, thus causing phase differences. In order to achieve a broadband achromatic metalens, the phase profiles with a fixed focal length over a wide range of wavelengths are required.

In recent years, Chen et al. [28], [29], [30] explained dispersion by introducing group delay and group delay dispersion into the phase profile as shown in (1). Equation (1) can be further expanded as a Taylor series near a design frequency ω_d as follows:

$$\varphi(r,\omega) = \varphi(r,\omega_d) + \left.\frac{\partial\varphi(r,\omega)}{\partial\omega}\right|_{\omega=\omega_d}(\omega-\omega_d) + \left.\frac{\partial^2\varphi(r,\omega)}{2\partial\omega^2}\right|_{\omega=\omega_d}(\omega-\omega_d)^2+\cdots. \tag{2}$$

The first term indicates that the wavefront of the incident light is a spherical wave. The second term depicts the time delay for different positions of the lens to reach the focus. The third term and higher ensure that the outgoing wavepackets are identical. The group delay describes how quickly the phase changes with frequency, which helps suppress chromatic aberrations over the entire wavelength range. The group delay can be derived from (1) for an achromatic metalens as:

$$\frac{\partial\varphi}{\partial\omega} = -\frac{1}{c}\left(\sqrt{r^2+f^2} - f\right). \tag{3}$$

The group delay is related to the spatial position when the focal length is irrelevant to ω. Meeting a certain distribution of phase and group delay is important to suppress chromatic aberration. It is worth noting that the group delay is determined by the geometry, adjacent pillars as well as pillar material properties. With C(ω) changing, φ(r, ω) will cause pillar redistribution in metalenses, which further affects the group delay profile of the metalens. C(ω) may provide an alternative chance to optimize the group delay and eliminate the chromatic aberration. Here, C(ω) is determined after obtaining the FLFC through a parametric sweep within 0$\sim$2π.

To demonstrate this concept, metalenses with different C(ω) are studied. The building block of the metalenses are circular silicon pillars with height and lattice period of 7.9 μm and 3.05 μm, respectively as illustrated in Fig. 1(a). Fig. 2(a) shows the relationship of phase shift and transmission with the pillar radius ranging from 300 nm to 1300 nm at a given design wavelength of 10 μm. The pillars cover 2π phase shift, and meanwhile maintain high transmittance, which is very beneficial to improve focusing efficiency. Fig. 2(c) shows the relative phase and group delay for the pillar with diameter D1 = 800 nm surrounded by different pillars shown in Fig. 2(b). The relative phase and group delay were obtained by changing adjacent pillars distribution of the pillar. One can see that the group delay of the pillars varies depending on the combination of the adjacent pillars while the relevant phase has no significant changes. Thus C(ω) can be considered as one dimension to optimize the group delay of the metalens to suppress the achromatic aberration, which hasn't been discussed before. The relative phase profile of the studied metalenses is achieved according to (1), where the aperture is 200 μm and the design focal length f is 480 μm. To quantitatively analyze the performance of chromatic aberration correction, the

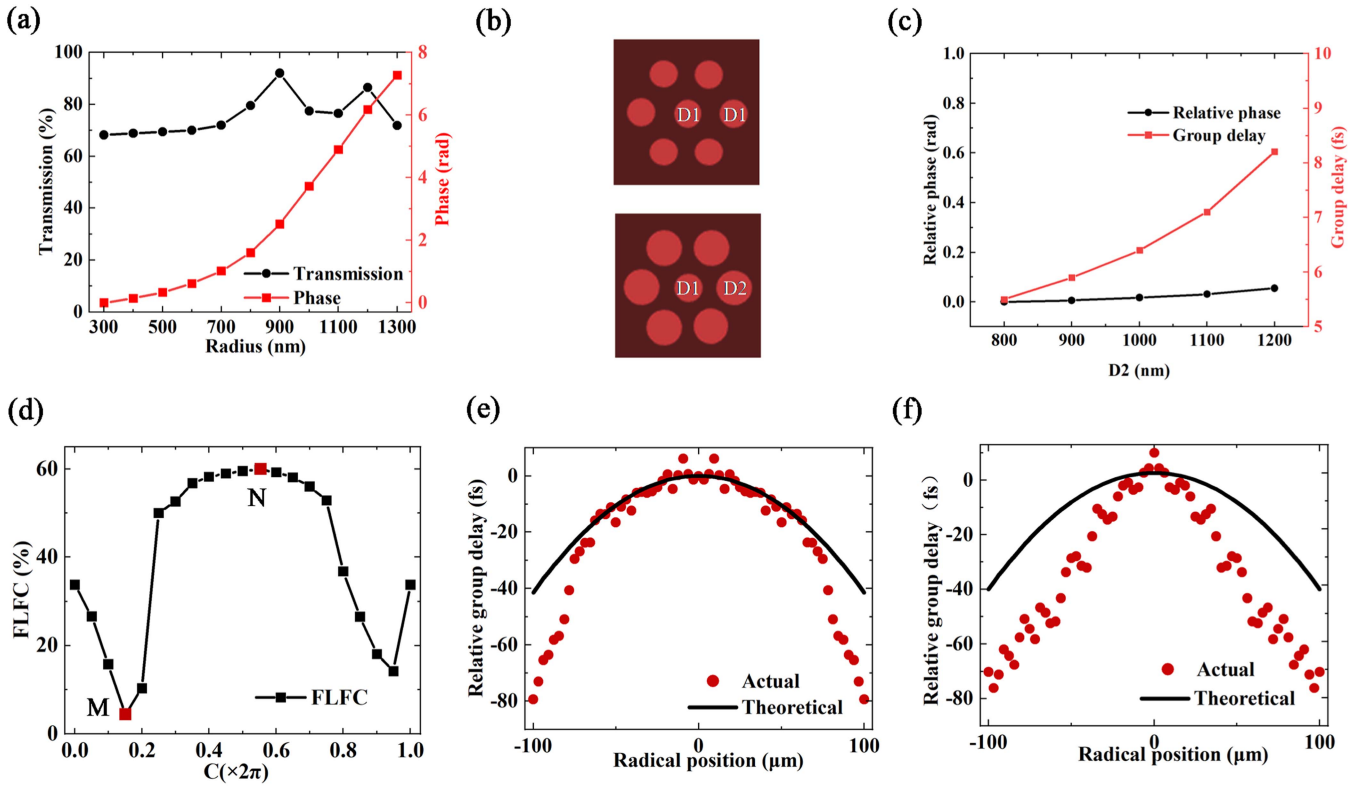

Fig. 2. (a) The transmission and phase as a function of pillar radius at 10 μm wavelength. (b) Schematic of pillars with the different surrounding pillars. (c) the relative phase and group delay of the pillar with diameter D1 = 800 nm surrounded by different pillars. (d) the FLFC of different C(ω). the minimum (4.1%) and maximum (59.8%) of the FLFC are marked as point M and N, corresponding to 0.15 $\times$ 2π and 0.55 $\times$ 2π of C(ω), respectively. (e-f) A comparison of the relative group delay for metalenses with the same diameter of 200 μm and NA of 0.24 but with different C(ω). the black solid line depicts the required theoretical group delay. The red dots are the actual group delay produced by the silicon pillars of the metalenses when C(ω) are the corresponding values of point M and N as illustrated in (d).

focal length fractional change (FLFC) is introduced as [22]

$$FLFC = \frac{f_{\max} - f_{\min}}{\text{mean}(f)} \times 100\%, \tag{4}$$

where $f_{\max}$, $f_{\min}$, mean(f) represent the maximum, minimum and average focal length over the interested bandwidth.

The FLFC presents the degree of focus shift deviation over the interested wavelength range. The smaller FLFC means the better achromatic performance of the lenses. It can be obtained using (4) to calculate after the metalens with different C(ω) are simulated. Fig. 2(d) shows the FLFC is a function of C(ω) in the design metalens, where M(C(ω) = 0.15 $\times$ 2π) and N(C(ω) = 0.55 $\times$ 2π) are the two points with the smallest FLFC of 4.1% and largest FLFC of 59.8%. Fig. 2(e), (f) show the comparison between actual group delay distribution of the metalens obtained by linearly fit the phase spectrum of the pillars in metalens and target group delay under the corresponding C(ω) value of M and N points in Fig. 2(d). The actual group delay of the metalens with C(ω) in M can approach to the target group delay, but significantly deviate with value in N. It can be seen the FLFC can be minimized to correct chromatic aberration by optimizing C(ω). It should be noticed as the larger diameters or NA of metalenses are required, the proposed method may meet some limitations since the larger group delay is required to compensate. A possible solution may need to introduce combined complex nano-structures to expand the group delay library.

Fig. 3(a) and (b) shows the electric field intensity distribution along the propagation direction of two metalenses with C(ω) corresponding to M and N in Fig. 2(d). Here we name the two metalenses as M metalens and N metalens, respectively. The dashed lines depict the average focal length of the metalenses working at wavelengths of 9 to 12 μm, and are defined as the effective focal plane of the metalenses. It can be seen that the suppression of chromatic aberration in M metalens is more superior that N metalens. Visible parasitic focal spots along the propagation direction are found mainly due to the imperfect match between the desired phase and the actual phase. Fig. 3(c) illustrates the normalized intensity profiles cut from the dashed line of M metalens. The full widths at half maximum (FWHM) on the focal plane are proportional to the operating wavelengths, increasing from 16.25 μm to 24.5 μm. The focal lengths and the chromatic focal shift sampled in the interested wavelengths are plotted in Fig. 3(d). The grey dashed line denotes the average focal length of 400.8 μm, yielding a simulation NA of 0.24. The deviation of the simulated average focal length from the design focal length (f = 480 μm) at 10 μm is possibly due to proximity effects between adjacent meta-atoms, and phase errors caused by the mismatch between the desired and actual phase responses of meta-atoms in a metalens. Chromatic focal

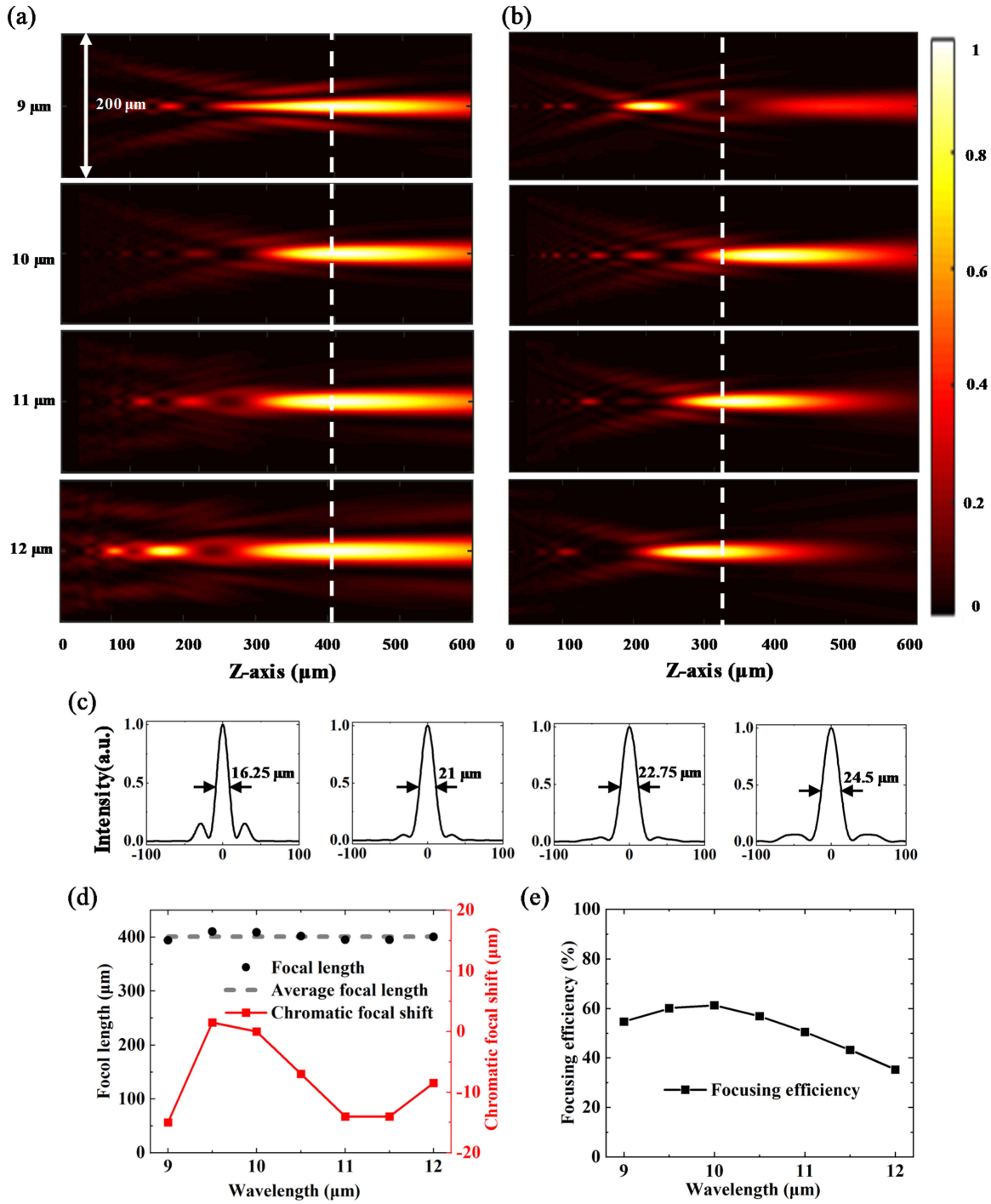

Fig. 3. Simulated normalized intensity distributions of metalenses with different C(ω), corresponding to (a) 0.15 $\times$ 2π. and (b) 0.55 $\times$ 2π. The average focal length is depicted by the dashed lines, corresponding to 400.8 μm and 312.2 μm. (c) Normalized intensity profiles along z-cut lines in the focal plane of the metalens in (a), Where the corresponding full widths at half maximum on focal plane is shown. (d) Simulated focal lengths and chromatic focal shift as a function of the sampled wavelengths. The grey dashed line depicts the average effective focal length of 400.8 μm. (e) Simulated focusing efficiency as a function of the sampled wavelengths.

shift shows the variation of focal lengths with wavelengths, referenced to the designed wavelength of 10 μm. The absolute value of the maximum chromatic focal shift is 15 μm. Fig. 3(e) shows that M metalens has focusing efficiency in a range of 35%$\sim$61% at the operation wavelengths of 9$\sim$12 μm. Correspondingly, the average focusing efficiency of 51.7% over the entire bandwidth is achieved. Focusing efficiency here is defined as the power fraction of transmitted light through a square aperture with a width of 72 μm positioned in the focal plane of the metalens and normal incident light (we assume the incident surface (non-metasurface layer) of the metalens is coated with anti-reflective layer, and has high transmittance of 100%). 72

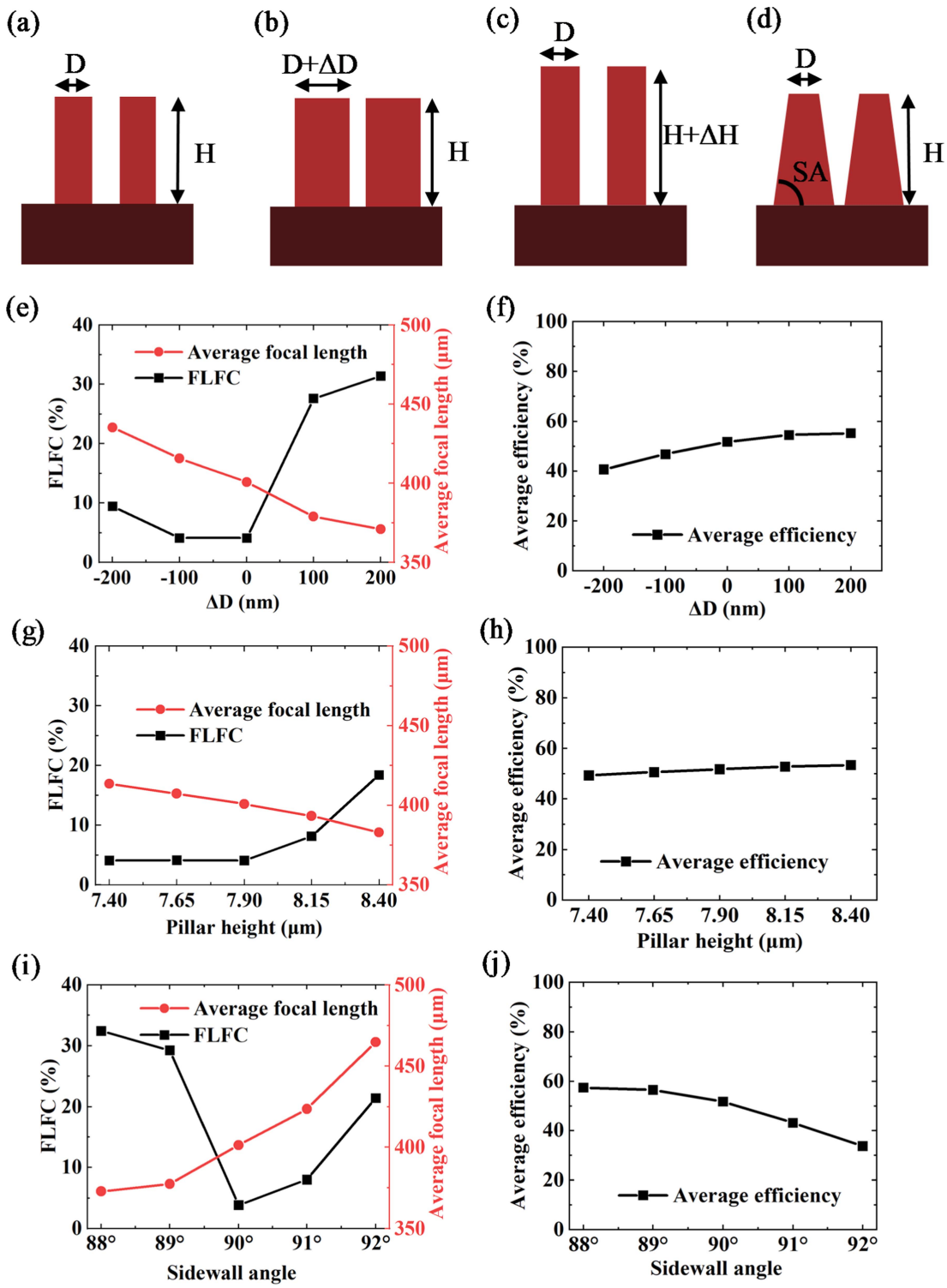

Fig. 4. Cross-sectional schematic of (a) Ideal nanopillars. (b) Nanopillars with a changed diameter (ΔD). (c) Nanopillars with a changed height (ΔH). (d) Nanopillars with a change sidewall angle (SA). (e-j) FLFC, average focal length and efficiency of different CD bias, pillar height and SA.

μm is selected as ~3 times of the max FWHM (24.5 μm) at 12 μm wavelength. Considering the practical applications, the pixel size of LWIR sensors is usually square, and thus the square integral area is proposed to use.

Precise phase modulation of light by metalenses comes from tailored design of subwavelength meta-atoms. While defects or errors during the fabrication process can have an effect on the geometry of the meta-atoms and thus influence the performance of a metalens. Deviations in critical dimension (CD) are common during CMOS fabrication process. Due to the non-uniformity of the etching process, the height of the pillars at the center and the edge of the wafer will deviate. It is difficult to maintain vertical

sidewalls for pillars with relatively large aspect ratio during etching process. Fig. 4(a)–(d) display cross-sectional schematic of ideal nanopillars, nanopillars with a changed diameter (ΔD), height (ΔH) and sidewall angle (SA), respectively. The influence caused by CD bias, pillar height variation and SA on the performance of the metalens can be analyzed by three metrics: the FLFC, average focal length and average focusing efficiency over the entire interested bandwidth. Additionally, this study applies uniform CD bias, height variation and SA on the whole nanopillars regardless of the individual dimensions.

One can see from Fig. 4(e) that CD bias has different effects on the FLFC over the interested wavelength range. The plus CD bias leads to a dramatic increase in FLFC, which causes the average focal length to decrease roughly linearly as a result. And the plus CD bias has a greater impact on FLFC than the minus CD bias. As the diameter changes, the transmission of a single pillar will also change, which will affect the average focusing efficiency of the metalens shown in Fig. 4(f). The impact on the average focusing efficiency is larger for the minus CD bias. When the diameter of pillars changes with ΔD as a whole, it is challenging to maintain the phase difference with the design wavelength, which is disadvantageous for an achromatic metalens. It can be seen that the small or large diameter of the pillar has a different effect on the performance of the achromatic metalens.

The influence of pillar height variation on the performance of the metalens is shown in the Fig. 4(g), (h). The FLFC remains almost unchanged when the height of the pillar is less than the design value but the average focal length is larger. However, the FLFC increases when the height of pillars is higher than the design value. It can be noticed that the higher pillar height, the smaller the effective focal length of the metalens, while there is not much effect on the average efficiency. When the height of pillars deviates, the phase response and transmission of a fixed diameter pillar for different wavelengths will also change. Here, the pillar height has a small effect on the average efficiency.

Non-ideal etching process normally gives rise to inclined sidewalls which lead to deviations in the phase response of nanopillars, resulting in changes in Chromatic aberration. As shown in Fig. 4(i), FLFC increases with the deviation of angled sidewall from the design angle (90°). The average focal length of the metalens ramps up while the average focusing efficiency drops with increasing of the SA. The performance deterioration may be caused by larger phase errors induced by slanted sidewall.

III. Conclusion

In summary, we propose and numerically demonstrate an achromatic metalens in a LWIR regime. Through exploiting the spectral degrees of freedom, the proposed metalens with a diameter of 200 μm and NA of 0.24 can achieve achromatic focusing over the wavelength of 9$\sim$12 μm with a FLFC of 4.1%. Our approach provides some advantages like reduced design complexity of unit structures to eliminate the achromatic aberration, compatibility of CMOS process and the realization of polarization insensitive metalens as the proposed nano-structures have fourfold rotational symmetry. Furthermore, we also analyze the influence of fabrication process deviation on the performance of the metalens. Our work provides a new way to design achromatic metalenses and may be promising for applications in infrared thermal imaging and miniaturized vision systems.

References

[1] J. S. Tyo, B. M. Ratliff, J. K. Boger, W. T. Black, D. L. Bowers, and M. P. Fetrow, "The effects of thermal equilibrium and contrast in LWIR polarimetric images," *Opt. Exp.*, vol. 15, no. 23, pp. 15161–15167, Nov. 2007.

[2] A. Dehzangi, J. Li, and M. Razeghi, "Band-structure-engineered high-gain LWIR photodetector based on a type-II superlattice," *Light. Sci. Appl.*, vol. 10, no. 1, Jan. 2021, Art. no. 17.

[3] H. X. Xu et al., "Tunable microwave metasurfaces for high-performance operations: Dispersion compensation and dynamical switch," *Sci. Rep.*, vol. 6, Nov. 2016, Art. no. 38255.

[4] F. Capasso, "The future and promise of flat optics: A personal perspective," *Nanophotonics*, vol. 7, no. 6, pp. 953–957, 2018.

[5] J. Engelberg and U. Levy, "The advantages of metalenses over diffractive lenses," *Nature Commun.*, vol. 11, no. 1, Apr. 2020, Art. no. 1991.

[6] N. Li et al., "Large-area metasurface on CMOS-compatible fabrication platform: Driving flat optics from lab to fab," *Nanophotonics*, vol. 9, no. 10, pp. 3071–3087, 2020.

[7] H. X. Xu et al., "Chirality-assisted high-efficiency metasurfaces with independent control of phase, amplitude, and polarization," *Adv. Opt. Mater.*, vol. 7, no. 4, 2018, Art. no. 1801479.

[8] C. Wang et al., "Heterogeneous amplitude−phase metasurface for distinct wavefront manipulation," *Adv. Photon. Res.*, vol. 2, no. 10, 2021, Art. no. 2100102.

[9] H. X. Xu et al., "Spin-encoded wavelength-space multitasking Janus metasurfaces," *Adv. Opt. Mater.*, vol. 2, no. 10, 2021, Art. no. 2100190, doi: 10.1002/adom.202100190.

[10] Z. L. Deng et al., "Diatomic metasurface for vectorial holography," *Nano Lett.*, vol. 18, no. 5, pp. 2885–2892, May 2018.

[11] Z. L. Deng et al., "Facile metagrating holograms with broadband and extreme angle tolerance," *Light Sci. Appl.*, vol. 7, 2018, Art. no. 78.

[12] G. Zheng, H. Muhlenbernd, M. Kenney, G. Li, T. Zentgraf, and S. Zhang, "Metasurface holograms reaching 80% efficiency," *Nature Nanotechnol.*, vol. 10, no. 4, pp. 308–312, Apr. 2015.

[13] H.-X. Xu et al., "Aberration-free and functionality-switchable meta-lenses based on tunable metasurfaces," *Appl. Phys. Lett.*, vol. 109, no. 19, 2016, Art. no. 193506.

[14] B. Li, W. Piyawattanametha, and Z. Qiu, "Metalens-based miniaturized optical systems," *Micromachines*, vol. 10, no. 5, May 2019, Art. no. 310.

[15] M. Khorasaninejad and F. Capasso, "Metalenses: Versatile multifunctional photonic components," *Science*, vol. 358, no. 6367, Dec. 2017, Art. no. eaam8100.

[16] M. Khorasaninejad, W. T. Chen, R. C. Devlin, J. Oh, A. Y. Zhu, and F. Capasso, "Metalenses at visible wavelengths: Diffraction-limited focusing and subwavelength resolution imaging," *Science*, vol. 352, no. 6290, pp. 1190–1194, Jun. 2016.

[17] H. X. Xu et al., "Polarization-insensitive 3D conformal-skin metasurface cloak," *Light Sci. Appl.*, vol. 10, no. 1, Apr. 2021, Art. no. 75.

[18] K. Zhang, Y. Wang, Y. Yuan, and S. N. Burokur, "A review of orbital angular momentum vortex beams generation: From traditional methods to metasurfaces," *Appl. Sci.*, vol. 10, no. 3, 2020, Art. no. 1015.

[19] S. Yu, L. Li, G. Shi, C. Zhu, and Y. Shi, "Generating multiple orbital angular momentum vortex beams using a metasurface in radio frequency domain," *Appl. Phys. Lett.*, vol. 108, no. 24, 2016, Art. no. 241901.

[20] M. I. Shalaev, J. Sun, A. Tsukernik, A. Pandey, K. Nikolskiy, and N. M. Litchinitser, "High-efficiency all-dielectric metasurfaces for ultracompact beam manipulation in transmission mode," *Nano Lett.*, vol. 15, no. 9, pp. 6261–6266, Sep. 2015.

[21] E. Arbabi, A. Arbabi, S. M. Kamali, Y. Horie, and A. Faraon, "Controlling the sign of chromatic dispersion in diffractive optics with dielectric metasurfaces," *Optica*, vol. 4, no. 6, pp. 625–632, 2017.

[22] M. Khorasaninejad et al., "Achromatic metalens over 60 nm bandwidth in the visible and metalens with reverse chromatic dispersion," *Nano Lett.*, vol. 17, no. 3, pp. 1819–1824, Mar. 2017.

[23] Z. Zhao et al., "Multispectral optical metasurfaces enabled by achromatic phase transition," *Sci. Rep.*, vol. 5, Oct. 2015, Art. no. 15781.

[24] M. D. Aiello et al., "Achromatic varifocal metalens for the visible spectrum," *ACS Photon.*, vol. 6, no. 10, pp. 2432–2440, 2019.

[25] W. T. Chen et al., "A broadband achromatic metalens for focusing and imaging in the visible," *Nature Nanotechnol.*, vol. 13, no. 3, pp. 220–226, Mar. 2018.
[26] W. T. Chen, A. Y. Zhu, J. Sisler, Z. Bharwani, and F. Capasso, "A broadband achromatic polarization-insensitive metalens consisting of anisotropic nanostructures," *Nature Commun.*, vol. 10, no. 1, Jan. 2019, Art. no. 355.
[27] W. T. Chen et al., "Broadband achromatic metasurface-refractive optics," *Nano Lett.*, vol. 18, no. 12, pp. 7801–7808, Dec. 2018.
[28] Z. B. Fan et al., "A broadband achromatic metalens array for integral imaging in the visible," *Light Sci. Appl.*, vol. 8, 2019, Art. no. 67.
[29] Z. Huang, M. Qin, X. Guo, C. Yang, and S. Li, "Achromatic and wide-field metalens in the visible region," *Opt. Exp.*, vol. 29, no. 9, pp. 13542–13551, Apr. 2021.
[30] B. Wang et al., "Visible-frequency dielectric metasurfaces for multiwavelength achromatic and highly dispersive holograms," *Nano Lett.*, vol. 16, no. 8, pp. 5235–5240, Aug. 2016.
[31] S. Wang et al., "A broadband achromatic metalens in the visible," *Nature Nanotechnol.*, vol. 13, no. 3, pp. 227–232, Mar. 2018.
[32] J. Chen, F. Zhang, Q. Li, J. Wu, and L. Wu, "A high-efficiency dual-wavelength achromatic metalens based on Pancharatnam-Berry phase manipulation," *Opt. Exp.*, vol. 26, no. 26, pp. 34919–34927, Dec. 2018.
[33] H. Yang et al., "High efficiency dual-wavelength achromatic metalens via cascaded dielectric metasurfaces," *Opt. Mater. Exp.*, vol. 8, no. 7, pp. 1940–1950, 2018.
[34] E. Arbabi, A. Arbabi, S. M. Kamali, Y. Horie, and A. Faraon, "Multi-wavelength metasurfaces through spatial multiplexing," *Sci. Rep.*, vol. 6, Sep. 2016, Art. no. 32803.
[35] O. Eisenbach, O. Avayu, R. Ditcovski, and T. Ellenbogen, "Metasurfaces based dual wavelength diffractive lenses," *Opt. Exp.*, vol. 23, no. 4, pp. 3928–3936, Feb. 2015.
[36] F. Aieta, M. A. Kats, P. Genevet, and F. Capasso, "Multiwavelength achromatic metasurfaces by dispersive phase compensation," *Science*, vol. 347, no. 6228, pp. 1342–1345, Mar. 2015.
[37] F. Balli, M. Sultan, S. K. Lami, and J. T. Hastings, "A hybrid achromatic metalens," *Nature Commun.*, vol. 11, no. 1, Aug. 2020, Art. no. 3892.
[38] F. Balli, M. A. Sultan, A. Ozdemir, and J. T. Hastings, "An ultrabroadband 3D achromatic metalens," *Nanophotonics*, vol. 10, no. 4, pp. 1259–1264, 2021.
[39] M. Meem et al., "Inverse-designed achromatic flat lens enabling imaging across the visible and near-infrared with diameter >3 mm and NA $= 0.3$," *Appl. Phys. Lett.*, vol. 117, no. 4, 2020, Art. no. 041101.
[40] S. Shrestha, A. C. Overvig, M. Lu, A. Stein, and N. Yu, "Broadband achromatic dielectric metalenses," *Light Sci. Appl.*, vol. 7, 2018, Art. no. 85.
[41] S. Wang et al., "Broadband achromatic optical metasurface devices," *Nature Commun.*, vol. 8, no. 1, Aug. 2017, Art. no. 187.
[42] Y. Wang et al., "High-efficiency broadband achromatic metalens for near-IR biological imaging window," *Nature Commun.*, vol. 12, no. 1, Sep. 2021, Art. no. 5560.
[43] K. Ou et al., "Mid-infrared polarization-controlled broadband achromatic metadevice," *Sci. Adv.*, vol. 6, no. 37, Sep. 2020, Art. no. eabc0711.
[44] K. Ou et al., "Broadband achromatic metalens in mid-wavelength infrared," *Laser Photon. Rev.*, vol. 15, no. 9, 2021, Art. no. 2100020.